Nanotechnology and Metal Nanoparticles for Wound Healing

Subjects: Dermatology

Contributor: Sara Sheikh-Oleslami , Brendan Tao , Jonathan D'Souza , Fahad Butt , Hareshan Suntharalingam , Lucas Rempel , Nafise Amiri

Wound healing is an intricate physiological process consisting of a series of molecular and cellular events that facilitate the regeneration of the skin, a protective barrier against the external environment. Since its inception, hydrogels have advanced the field of wound healing, insofar as to promote damaged tissue healing within a hydrated milieu. As well, the integration of therapeutic nanoparticles (NP) and biomolecules into hydrogels for local wound application has been shown to enhance and accelerate healing.

nanoparticles nanotechnology wound healing antimicrobial agents hydrogels

1. Nanotechnology for Wound Healing

Nanotechnology is defined as the manipulation of materials on an atomic or molecular scale [1]. Ever evolving, nanotechnology has revolutionized many industries, especially within the fields of nanoscience, nanoparticles, nanomaterials, and nanomedicine. Specifically, the field of nanomedicine has risen in popularity with myriad applications, including vaccine production, wearable devices, implants, drug delivery, and antibacterial applications [2]. In tissue engineering and regenerative medicine, nanomaterials have shown low toxicity and customizability, making them versatile agents to incorporate into medical practice [2]. For instance, metal nanoparticles such as silver (Ag) [3], gold (Au) [4], copper (Cu) [5], and zinc oxide (ZnO) [6] have demonstrated marked antimicrobial properties. While these intrinsic properties are advantageous for wound healing, these metal nanoparticles can also display anti-infective properties within drug-delivery vehicles.

2. Nanoparticles Used in Wound Healing

Metal nanoparticles have been considered in clinical applications for reasons including small size, high surface-to-volume ratio, shape, stability, low toxicity, and economic reasons, given their affordability [7][8]. Additionally, they can conveniently integrate into wound dressings [7]. One of the primary mechanisms in which antibacterial activity is offered by metal nanoparticles is through their bacteriostatic properties via attachment to DNA or RNA, via electrostatic interactions, halting further replication [9]. MicroRNAs, short, non-coding RNA molecules that have regulatory roles in gene expression, play a large role in wound healing processes, including inflammation, angiogenesis, cell proliferation, and ECM remodeling. In aberrant wound healing, such as infectious states, microRNAs can be targeted by metal nanoparticles through encapsulation, shielding charge groups and allowing

for cellular uptake [10]. The modulation of microRNA allows for the enhancement of gene expression factors, promoting the production of factors essential for wound healing. Further, targeted delivery of these therapeutic agents minimizes off-target effects [10].

Another mechanism is through bactericidal properties via the creation of reactive oxygen species [9]. When embedded in hydrogel scaffolds, a substitute is created for damaged ECM which facilitates fibroblast proliferation and matrix formation for enhanced regeneration and repair [11][12]. As such, these nanoparticles can be used in lieu of antibiotics and are thought to accelerate and ameliorate healing while preventing infection [7][8]. A graphical summary of wound healing mechanisms per nanoparticle is depicted in **Figure 1**.

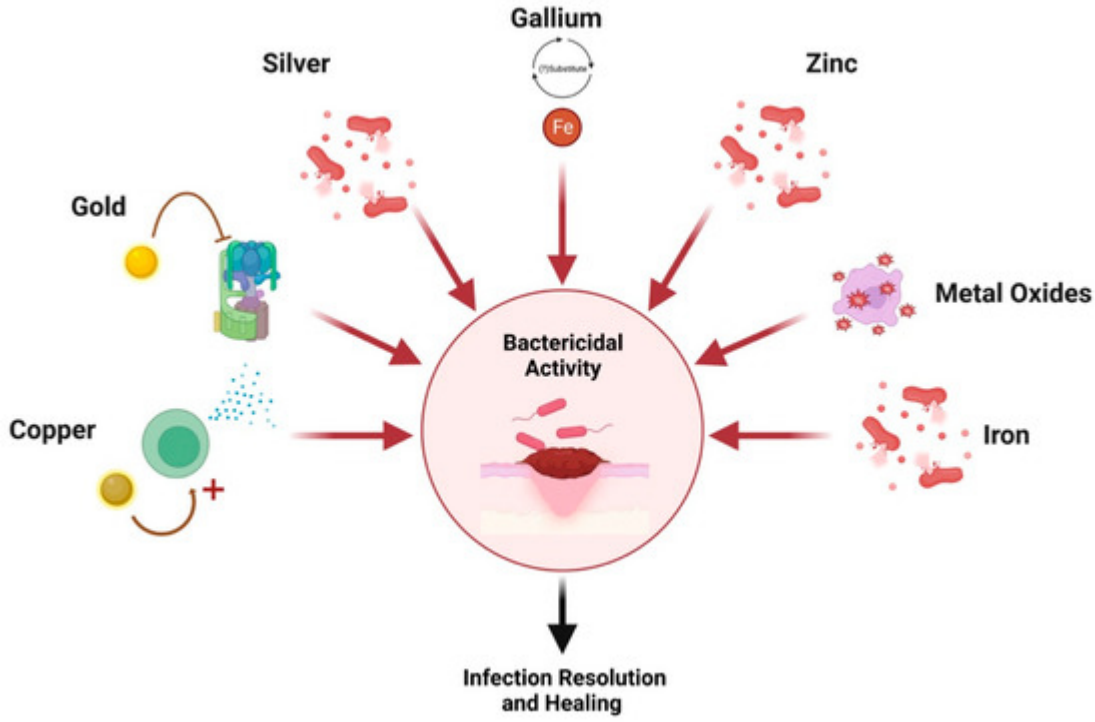

Figure 1. Nanoparticle mechanisms of action. Created with Biorender.com.

2.1. Silver (Ag) Nanoparticles

The use of silver for the treatment of wounds and infection prevention dates back to at least 4000 B.C.E. with documented medical applications dating back to the 1700s; however, in large quantities, silver can also impair healing due to its toxic effects on keratinocytes and fibroblasts [13][14]. Today, silver continues to serve many applications in wound healing. For example, silver nitrate is used as a commonplace treatment for chronic wounds while silver sulfadiazine is used for burns. Nanotechnology has changed the use of silver for wound healing with the creation of silver nanoparticles (AgNPs), which are the most commonly used metal nanoparticles in wound management with many applications, including wound infections, ulcers, and burns. Known for their wide range of antimicrobial activity, effective against bacteria, viruses, fungi, and protozoa, as well as promotion of wound healing, AgNPs have been shown to disturb quorum sensing, effectively reducing biofilm formation [15][16][17].

The antibacterial effect is demonstrated via bactericidal and inhibitory mechanisms. In terms of bactericidal activity, apoptosis is induced in bacteria through AgNP interactions with sulfur and phosphorous-containing proteins, effectively disrupting cell membranes [18]. Moreover, as DNA consists of sulfur and phosphorous, AgNPs act on these bases to destroy DNA, further facilitating the apoptosis of bacterial cells [18]. Moreover, the continuous release of AgNPs, specifically at lower pH whereby acidic environments facilitate the oxidation of AgNPs to Ag^+, negatively charged proteins are bound to, allowing for disruption of bacterial cell walls and membrane [18]. Through this mechanism, cell respiration is also disrupted through damage to bacterial mitochondria [19][20]. Despite these cytotoxic effects, which are AgNP-dose- and size-dependent, the proliferation of fibroblasts and keratinocytes is not affected [21]. In terms of inhibitory mechanisms, the presence of AgNPs in the wound environment allows for the formation of reactive oxygen species (ROS), which further disrupt bacterial cell viability through oxidative stress [19][20]. Wound healing is accelerated through these antibacterial properties as microbes can delay all stages of wound healing.

In addition to the antimicrobial properties of AgNPs, they also promote wound healing [22][23][24][25]. Firstly, they assist in the differentiation of fibroblasts into myofibroblasts, which allows for wound contractility [26]. Moreover, they stimulate the proliferation and relocation of keratinocytes to the wound bed [27]. As such, quicker wound epithelialization and scarless wound healing are promoted [26]. Accelerated and complete healing with increased epithelialization was observed in a study wherein an AgNP hydrogel was applied to a partial-thickness cutaneous wound in mice [28][29].

AgNPs also have anti-inflammatory effects through cytokine modulation, reducing levels that allow for decreased lymphocyte infiltration, further enhancing re-epithelialization [5][30]. One study demonstrated a significant reduction in inflammatory cytokines and oxidative stress, effectively promoting healing, while another study in a burn wound model in mice demonstrated reduced interleukin-6 (IL-6) and neutrophils and increased the levels of IL-10, vascular endothelial growth factor, and TGF-ß [3].

The summary of all in vivo studies related to AgNP-loaded hydrogels is shown in **Table 1**.

Table 1. Summary of Characteristics and Findings of Included Trials for Silver Nanoparticles.

Hydrogel Species	Particle Size (Diameter)	Dosage of NP	Rate of Release	Antimicrobial Capability	Cell Type	Cytotoxic Effect	Animal Model	In Vivo Findings	Year	Source
Polyvinyl Alcohol (PVA)	74.58 nm	10% *w/v*	-	Minimum inhibitory concentration 3.13 ug/mL for *E. coli* and 25 ug/mL for *S. aureus*	-	-	Full-thickness wounds in rabbits	Wound closure is accelerated with AgNP (12–14 days) compared to control with marketed drug (23 days)	2019	[31]
PVA and Cellulose	10–200 nm	1000 ppm	~42% after 48 h	More effectively inhibits *S.*	-	-	Full-thickness	Faster healing with minimum	2016	[32]

Hydrogel Species	Particle Size (Diameter)	Dosage of NP	Rate of Release	Antimicrobial Capability	Cell Type	Cytotoxic Effect	Animal Model	In Vivo Findings	Year	Source
				aureus compared to *E. coli* (92% bacterial reduction)			wound in mice	scarring was seen in the AgNP group		
Chitosan	10–20 nm	0.1 mg/g	Constant at regular time intervals	Inhibition zone: *Pseudomonas aeruginosa*: 21.47 ± 0.50 mm; *Bacillus cereus*:11.52 ± 0.19 mm *Staphylococcus aureus*: 19.97 ± 0.73 mm; *Escherichia coli*: 17.30 ± 0.03 mm; *Klebsiella pneumonia*: 15.50 ± 0.51 mm	Human leukemia cell lines (THP1)	Nontoxic with an IC50 of 151.10 µg/mL at 24 h	*P. aeruginosa* infected excisional wound model in rats	Faster healing with better scar appearance in AgNP group with lower bacterial counts and enhanced connective tissue production compared to control	2021	[33]
Guar gum	8.24 ± 4.20 nm	<0.200 nM	-	Day 12 post-incision colony count (cfu): AgNPs: 20 cfu; commercial antibacterial gel (control): 51 cfu	Human dermal fibroblast cells	Low cytotoxicity with 80% cells viability	Full-thickness wounds in rats	>40% wound healing and 60% antibacterial activity compared to commercial antibacterial gels	2021	[34]
Poly (ethylene glycol) diacrylate (PEGDA)	-	5, 25, and 30 mg/mL	15.2% Ag^+ released in 4 h	Bacterial viability of *E. coli* and *S. aureus* after 5–10 min of NIR laser exposure is 0 Inhibition zone: 0 mm	L929 fibroblast cells	>90% cell viability for all groups other than the groups with 50 mg/mL	*S. aureus infected* excisional wound model in rats	Good sustained anti-bacterial effects observed with greater wound healing response in experimental group 7 days after treatment	2022	[35]
Polyacrylic acid	-	0.1% *w/v*		Effective against *S. aureus* and *E. coli*	Murine fibroblast 3T3 cells	Proliferation promoted; low toxicity and good cell viability	Full-thickness wound model in diabetic mice	97% wound reduction compared to 81% wound reduction for control on day 14	2022	[36]

Hydrogel Species	Particle Size (Diameter)	Dosage of NP	Rate of Release	Antimicrobial Capability	Cell Type	Cytotoxic Effect	Animal Model	In Vivo Findings	Year	Source
Chitosan and gelatin	20–80 nm; mean 36 nm	1% *w/v*	-	Highest biofilm eradication noted against *S. aureus* and *P. aeruginosa* with AgNP (89 ± 5%)	Mouse embryonic fibroblasts	Low toxicity	Excisional wound splinting model in BALB/c mice	Accelerated and ameliorated wound healing compared to control with enhanced angiogenesis, collagen synthesis, and sebaceous gland/hair follicle regeneration	2022	[37]
PF127 polymer	33 nm	0.1, 0.3, and 1.0 mg	-	Zone of Inhibition: *Bacillus cereus* (17.7 mm), *Escherichia coli* (18.7 mm), *Pseudomonas aeruginosa* (10.3 mm), and *Staphylococcus aureus* (17.7 mm) Minimum inhibitory concentration and minimum bactericidal concentration: 390–780 µg/mL	Drosophila melanogaster eggs	No significant effect on eclosion of F1 flies for doses under 250 micrograms/mL of AI-AgNPs	Full-thickness excisional wound model in mice	In a concentration-dependent manner, the wound contraction for the treatment groups were higher than for the control group; no skin irritation observed in patch test	2021	[38]
Chitosan	20–35 nm	-	Continuous with release co-efficient of 0.37	Zone of Inhibition: *E. coli*: 13.6 ± 0.3 mm; *B. subtilis*: 10.5 ± 0.8 mm; *P. aeruginosa*: 9.2 ± 0.3 mm; *S. aureus*: 11.4 ± 0.1 mm	-	-	Full-thickness excisional wound model in diabetic rats	The rate of wound contraction was higher compared to the control. Scar-free regeneration of the skin with intact patches of hair growth was also noted with the AgNP treatment	2021	[39]
Polyvinylpyrrolidone (PVP), polyethylene glycol (PEG),	31 nm	-	-	-	NCTC L929 cell line	Non-cytotoxic	Full-thickness excisional	Stimulatory action on wound healing as evidenced by a high intensity of	2018	[40]

Hydrogel Species	Particle Size (Diameter)	Dosage of NP	Rate of Release	Antimicrobial Capability	Cell Type	Cytotoxic Effect	Animal Model	In Vivo Findings	Year	Source
carboxymethyl cellulose (CMC)							wounds in rabbits	fibroblasts and neovascularization in the tissue, which promoted a faster healing process when compared to the untreated wounds		
Gelatin	68.5 nm	200 μg/mL	With irradiation: 39.24%; without: 29.92% after 30 min	22.46% of methicillin-resistant *Staphylococcus aureus* (MRSA) and 24.48% of *E. coli* were eliminated compared to 22.46% and 20.37% in the control without irradiation. With irradiation, 97.57% of MRSA and 95.99% *E. coli* were killed due to photothermal effects of AgNPs	HaCAT cells	At <250 μg/mL, cell viability >80%, however cell viability decreased with increased concentration	MRSA-infected wound model in mice	91.76% of MRSA in wounds was removed with improved healing, angiogenesis, and collagen deposition.	2021	[41]
Lignin and cellulose	100 nm	3, 6, 9, 12% *w/v*	-	When in contact with the 12% *w/v* AgNP hydrogel for 2 h, *E. coli*, *S. aureus*, *C. albicans*, and *MRSA* had no colonies on the agar plates, indicating that all bacteria that were in contact with the hydrogels were killed	Mouse L929 fibroblast cells	Survival rate of cells in each concentration group was >90%	Full-thickness excisional wound infected with MRSA in rats	The hydrogels can maintain a moist healing environment, reduce inflammatory cell infiltration, promote M2 macrophage polarization, accelerate collagen deposition, promote angiogenesis, and accelerate wound healing of MRSA-infected wounds.	2021	[42]

Hydrogel Species	Particle Size (Diameter)	Dosage of NP	Rate of Release	Antimicrobial Capability	Cell Type	Cytotoxic Effect	Animal Model	In Vivo Findings	Year	Source
Alginate and Gelatin	7.5–8.3 nm at 1 mM, 20–34 nm at 4 mM	1.0, 2.0, 40.0 nM	-	**Minimum Inhibitory Concentration**: 0.50 µg/mL against *Pseudomonas aeruginosa* and 53.0 µg/mL against *Staphylococcus aureus* at 4 nm	Human L929 fibroblasts	96% cell viability observed at 4 mM	Full-thickness excisional wound model in rats	Accelerated wound healing, earlier development, and maturation of granulation tissue	2020	[43]
Hydroxypropyl methylcellulose	40–70 nm	10, 20, 40, 80 µg/mL	-	Inhibition zone increased with increasing concentration. At 80 µg/mL: *E. coli*: 20 mm; *S. aureus*: 19 mm	-	-	Full-thickness excisional wounds in rats	The percentage wound healing for formulation was 9.34% more than that of standard (silver sulfadiazine cream) at day 14 with accelerated wound contraction and reduced epithelialization periods, however, the standard showed 1.78% higher healing on day 21.	2014	[44]
Zwitterionic poly (sulfobetaine methacrylate) monomer and protected dopamine methacrylamide monomers (DMA) hydrogel	18 ± 2 nm	2 mM	46 µg/L for a 5 × 5 cm^2 sample during the first day and gradually increased thereafter	Inhibition Zone: 157, 148 and 129% for *E. coli*, *S. aureus*, and *P. auregenosa* compared to control. Less significant effect on Gram-positive than -negative bacteria. Suspension assays measuring the optical density (OD) of bacteria at 600 nm show	MC3T3-E1, Human HS68/F3T3 Fibroblasts	Due to the low concentrations of silver released, Mammalian cell viability was not greatly affected during 5 days of incubation	Full-thickness excisional wounds in rats	The percentage of the wound size reduction was 59% for the control, 80 for the hydrogel alone, and 98% for the AgNP-hydrogel treatment	2016	[45]

Hydrogel Species	Particle Size (Diameter)	Dosage of NP	Rate of Release	Antimicrobial Capability	Cell Type	Cytotoxic Effect	Animal Model	In Vivo Findings	Year	Source
				significantly decreased OD values in AgNP group in comparison to other samples, demonstrating bactericidal effects						
Pluronic F127	2.6 nm	200 µg/g	Initial burst during the first 10 h, followed by a sustained release over 24 h	AgNPs reduced *S. aureus* viability by up to 77% compared to 50% in SSD and 20% in the blank hydrogel Zone of Inhibition: AgNP hydrogel: 14 mm; SSD: 11 mm; blank hydrogen: 7 mm	-	-	*S. aureus* infected full-thickness excisional wound model in	AgNP hydrogel to the wound provides superior bactericidal activity and reduces inflammation leading to accelerated wound closure when compared to industry-standard silver sulfadiazine. It also accelerated wound closure and improved wound re-epithelialization. Further, decreased neutrophil infiltration, increased anti-inflammatory Ym-1 positive M2 macrophages, and reduced the number of caspase-1 positive apoptotic cells were also observed.	2021	[46]
Chitosan and Konjac Glucomannan	60 nm	200 µg/mL	Release in a gradual manner	Superior ability for AgNPs-loaded hydrogels to kill *S. aureus* and *E. coli.*	L929 cells	95% cell survival rate	*S. aureus* infected full-thickness wounds in rats	Promotes accelerated infected wound repair with no adverse reactions or symptoms	2020	[47]

Hydrogel Species	Particle Size (Diameter)	Dosage of NP	Rate of Release	Antimicrobial Capability	Cell Type	Cytotoxic Effect	Animal Model	In Vivo Findings	Year	Source
Riclin	25.92 nm	1.0 mM	Sustained released with complete release observed at 48 h	Inhibitory concentration of *S. aureus* was 10 µg/mL and *E. coli* was 10 µg/mL	Mouse skin fibroblast (NIH3T3) cells and macrophage (Raw 264.7) cells	Weak cytotoxicity (>60% cell viability) toward NIH3T3 mouse fibroblasts at concentrations of 54 µg/mL	*S. aureus* infected full-thickness wounds in mice	Faster wound healing, more complete re-epithelialization, and denser collagen deposition characteristics.	2022	[48]
Chitosan	-	6, 12, 24, 48 mM (24 being the optimum dose)	After 12 h co-culture, concentrations of 3.01, 3.92, 6.62, and 8.26 mg/L were obtained with Ag^+ doses of 6, 12, 24, and 48 mM, respectively	Significant bactericidal effects noted MPI: *S. aureus*: 35% and *S. epidermis:* 34%	NIH/3T3 cells and KERTr cells	Cell viability could be maintained >90% when the concentration of Ag^+ in the HTM was <6 mg/L	Full-thickness wounds in diabetic rats	Higher wound closure efficiency and faster recovery of integrity and functionality of the newly formed tissues compared to other treatments	2021	[49]
Gelatin	300 nm	1 mg/mL	Quick release during the first 48 h, reaching 29.65% In the following stage, prolonged-release profiles over 504 h (21 days) were observed, with a cumulative percentage of 61.37%	A sustained antibacterial effect was observed against *E. coli* and *S. aureus* compared to no bacteriostatic ability in the pure hydrogel alone.	MC3T3-E1	Good cell compatibility observed	Scalded skin model to produce 2-degree burns in rats	Only 15% of the wound area left on day 10. Histology results showed the epidermal and dermal layers were better organized compared to the control.	2022	[50]
Lignocellulose	-	0.5 and 0.8% *w/v*	pH-dependent release	4.1% survival rate for *S. aureus* and 2.9% survival rate for *E. coli*	L929 fibroblast cell line	>95% of the cells are viable after 36 h incubation. No hemolytic activity observed.	*S. aureus* infected full-thickness wounds in mice	Significantly accelerate tissue regeneration and wound healing process through increasing collagen deposition and decreasing inflammation while retaining excellent biocompatibility	2021	[51]

Hydrogel Species	Particle Size (Diameter)	Dosage of NP	Rate of Release	Antimicrobial Capability	Cell Type	Cytotoxic Effect	Animal Model	In Vivo Findings	Year	Source
Cellulose and gelatin	-	0.2 and 0.5 mg/mL	-	Decrease in *S. aureus* and *P. aeruginosa* activity Inhibition zone: ~2 mm at 0.5 mg/mL	Neonatal human dermal fibroblasts (NHDF)	CNF/G/Ag0.5 presented highest satisfactory infected cell viability (>100%)	Full-thickness wounds in mice	The CNF/G/Ag groups had much declined size of the wound than the control; wounds treated with CNF/G/Ag0.5 healed ~90% after treated Bacterial infection of the wound was reflected by weight loss. Treatment with CNF/G/Ag0.5 displayed a clear advantage in survival rate (83.3%)	2018	[52]
Aloe vera-silk fibroin composite	40 nm	0.5 mg/mL	pH-dependent release: 40.89% release in neutral environment, and 55.12% in acidic environment	Antibacterial rings presented in the AgNP hydrogel had the largest diameter both for *E. coli* (13.92 ± 0.94 mm) and *S. aureus* (10.623 ± 0.61 mm), demonstrating superior antibacterial properties	L929, Mesenchymal Stem Cells	Promotion of cell proliferation and migration; good biocompatibility	Full-thickness excisional wounds in rats	Accelerating healing and inhibition of immune reactions observed with better performance in early inflammatory response stages. Good antibacterial properties, satisfactory biocompatibility and promotes cell proliferation, migration, and wound healing in the AgNP hydrogel compared to the controls.	2021	[53]
Cellulose	119.7 ± 5 nm (natural cashew gum—NCG); 123.8 ± 8.9	NCG: 36 × 10^{10} particles/mL PhCG: 4.03 × 10^{10} particles/mL	-	Antibacterial activity was tested against *S. aureus* and *P. aeruginosa*. The hydrogel base alone did	-	-	Full-thickness wounds in rats	Improved healing was observed compared to the control	2017	[54]

Hydrogel Species	Particle Size (Diameter)	Dosage of NP	Rate of Release	Antimicrobial Capability	Cell Type	Cytotoxic Effect	Animal Model	In Vivo Findings	Year	Source
	nm (phthalated cashew gum—PhCG)			not present an antimicrobial effect. The effect of the hydrogels was more effective *against P. aeruginosa*, whereas the PhCG-AgNP was more potent than the NCG-AgNPs. For the gram-negative bacterium, the MIC values presented the same value of MBC for both hydrogels, which indicates a bactericidal effect. Hydrogels with AgNPs showed lower MICs when compared to the effect of $AgNO_3$ solutions at the same concentrations tested for the two bacteria.						
Cellulose	28 nm	-	2.0% *w/v*	Good resistance against Gram-positive and Gram-negative bacteria, with *E. coli* and *S. aureus* showing superior colony formation suppression. Bacterial death	-	-	*S. aureus* infected full-thickness wounds in rats	Accelerated wound healing with superior antibacterial and wound healing properties noted. Significantly improved wound closure by day 16, and histological examination of the tissue in the	2022	[55]

Hydrogel Species	Particle Size (Diameter)	Dosage of NP	Rate of Release	Antimicrobial Capability	Cell Type	Cytotoxic Effect	Animal Model	In Vivo Findings	Year	Source
				was recorded in 78.9 ± 2.61% of the cases in the control and 95.6 ± 1.93% in the presence of AgNPs				wounded area showed rapid reepithelialisation, differentiated dermis, and epidermis, with minimal scar tissues.		
Silk fibroin	-	5% *w/v*	Rate of release of AgNP varies depending on metformin-loaded mesoporous silica microspheres (MET@MSNs): Ag NPs mass ratios	Colony counts reduced from 7.72 ± 0.10 (CFU/mL) to 6.90 ± 0.09 (CFU/mL) for *S. aureus* and from 7.15 ± 0.09 (CFU/mL) to 6.30 ± 0.43 for *E. coli*. Zones of inhibition for *S. aureus* and *E. coli* are comparable to antibiotic-sensitive tablets	RAW264.7, EA.hy926, and L929 cells	For RAW264.7 cells, >90% cell viability on day 7 with hydrogel application [75][76]	Full-thickness excisional wounds in diabetic mice [77]	Rapid wound healing was observed regeneration of squamous epithelium, collagen formation, and angiogenesis indicative of good wound repair compared to control	2022	[56]
Carbopol	21 nm [79]	100 µg/g	-	Microbicidal activity on *S. aureus* and *E. coli* with MBC close to 100 µg/ mL, and MtE has a microbicidal response on *S. aureus* with MBC of 50 µg/mL. Besides, AgMt NPs-G produces a marked bacterial inhibition by contact in both strains	HUVEC cells	MtE and AgMt NPs tested concentrations for toxicity do not show an important effect on cell viability, except for AgMt NPs 100 µg/mL concentration, where cell viability falls by almost 10% [80][81]	Second-degree burn injuries in rats	Higher wound healing ratio and faster wound evolution compared to control.	2021	[57]

nds due
fects are
nhibitory.
collapse
cell [78].
ze of the
stronger
mmatory
seen as
AuNPs are able to bind free radicals such as nitric oxide (NO) or hydroxyl (OH$^-$) [82][83][84]. This strong catalytic activity in free radical scavenging is further observed through the ability of AuNPs to increase nuclear factor erythroid 2-related factor (NRF2), which allows for antioxidant gene activation [85][86]. Furthermore, while being able to facilitate the creation of ROS, they are also able to receive electrons and remove or deactivate ROS, with greater effects seen the higher the surface area of the AuNPs is [76].

In addition to tissue repair, wound healing is found to be accelerated and ameliorated with the use of AuNPs through the promotion of collagen expression, growth factors, vascular endothelial growth factor (VEGF), fibroblast proliferation, decreased cellular apoptosis, and angiogenesis [20][87].

Despite these beneficial effects, AuNPs must usually be incorporated with other biomolecules for efficacy in wound healing applications. Examples include the incorporation of AuNPs in chitosan or gelatin for the enhancement of wound healing or in collagen for a similar effect [4][5]. One study of a rat full-thickness excisional wound model demonstrated accelerated healing and wound closure with improved hemostasis and re-epithelization compared to the Tegaderm dressing and pure chitosan hydrogel controls in a chitosan-AuNP hydrogel [88]. Recent studies have also incorporated phototherapy in conjunction with AuNPs to achieve antimicrobial activity [6][89].

Hydrogel Species	Particle Size (Diameter)	Dosage of NP	Rate of Release	Antimicrobial Capability	Cell Type	Cytotoxic Effect	Animal Model	In Vivo Findings	Year	Source
				AgNP-impregnated chitosan hydrogels have better						
Hydrogel Species	**Particle Size (Diameter)**	**Dosage of NP**	**Rate of Release**	**Antimicrobial Capability**	**Cell Type**	**Cytotoxic Effect**	**In Vivo Model**	**In Vivo Findings**	**Year**	**Source**
Cydonia oblonga seed extract	20–30 nm	10 mmol	-	MIC: *B. simplex*: 16 mg/mL; *B. subtilis:* 32 mg/mL; *P. aeruginosa:* 32 mg/mL; *E. coli*: 16 mg/mL; *S. aureus:* 40 mg/mL; *A. niger:* 50 mg/mL; *P. notatum*: 50 mg/mL Inhibition zone: *B. Simplex:* 15 mm; *B. Subtilis:* 17 mm; *P. aeruginosa*: 16 mm; *E. Coli:* 18 mm; *S. Aureus*: 12 mm	-	-	Full-thickness wounds in mice	99% wound closure in 5 days; increased expression of NANOG and CD-4 in nanoparticle treatment group	2022	[90]
Alginate	25 nm (NP), 50, 70, 120 nm spike length (nanostars (NS))	1.5 µg/mL	NP: 157 ng release over 12 h; NS: 8.63 ng release over 12 h	The bacterial killing of >95% is observed for *P. aeruginosa* and *E. coli*, while up to 60% for Gram-positive *S. aureus*. >80% of colonies of *P. aeruginosa* and *E. coli* were also reduced.	NIH-3T3	85% viability	*S. aureus* infected full-thickness wounds in rats	Accelerated wound healing with enhanced wound closure and angiogenesis	2022	[91]

Hydrogel Species	Particle Size (Diameter)	Dosage of NP	Rate of Release	Antimicrobial Capability	Cell Type	Cytotoxic Effect	In Vivo Model	In Vivo Findings	Year	Source
				35.4% reduction of colonies were obtained for *S. aureus*.						
Poloxamer	29.2 ± 2.1 nm	-	Slow and prolonged release over 48 h, ~2%/min	High percentage reduction of bacterial viable count against *S. aureus* and *P. aeruginosa*	-	-	Full-thickness excisional wound model in rats	Almost completely healed wound after 14 days of daily treatment compared to control, owing to their enhanced skin re-epithelization effect and collagen formation, in addition to their impact on the gene expression of inflammatory and anti-inflammatory mediators. Furthermore, low percentages of deposition into the main body organs after 21 days of daily wound treatment was seen.	2019	[92]
Polyethyleneimine (PEI), polyethylene glycol (PEG), hexachlorocyclic triphosphonitrile (HCCP)	22 nm	0.3, 3, 5 nM	Release ratio of approximately 70% after 16 h incubation with the tendency to	Improved performance against *S. aureus* and MRSA, especially if the gel is exposed to	L929 cells	Negligible cytotoxicity, good biocompatibility, and excellent hemocompatibility	Full-thickness excisional wound model in mice	Accelerated wound healing with no toxicity or significant adverse effects	2022	[93]

2.3. Copper (Cu) and Copper Oxide (CuO)

Hydrogel Species	Particle Size (Diameter)	Dosage of NP	Rate of Release	Antimicrobial Capability	Cell Type	Cytotoxic Effect	In Vivo Model	In Vivo Findings	Year	Source
			slow down thereafter	laser irradiation	[96][97][98][99][100][101]			compared to the control.		
Alginate	- [106][107]	0.05, 0.1, 0.2 mg/mL [104][105]	In PBS (pH 7.2–7.4, 0.1 M), approximately 74%, 73%, and 76% of Ga^{3+} was released from Ga^{3+}-crosslinked hydrogel	Strong bactericidal activity against *S. aureus* and *P. aeruginosa* observed with higher reduction in *P. aeruginosa* compared to *S. aureus*. Faster release of silver ions demonstrated stronger antibacterial effect. [110]	Keratinocytes (HaCaT) [102] [103]	After 1, 3 and 7 days of incubation, the materials did not show any toxicity even after 7 days of contact and up to 96% of keratinocytes were viable	Full-thickness wounds in diabetic and non-diabetic mice	Rapid contraction of wound edges was seen in comparison to the controls as well as minor scab formation and lack of inflammation in the integument. Fifteen days of treatment with the nano-enabled hydrogels completely recovered the wounds of non-diabetic and diabetic mice. The bactericidal effect was also evidenced by absence of bacterial contamination in the wounds. [5]	2021 [108][109] [111]	[94]
Chitin	215.31 nm	2.5, 5, 10% w/v [112][113]	-	Hydrogels with Au contents of 5% and 10% were most effective at inhibiting *E. coli* growth, whereas a content of >2.5% was	L929 cells	The survival rate of cells in all concentrations of Au was >80% at 2 h, and even over >90% in most groups. At 48 h, except for the 10% group, the cell viability of	*S. aureus* infected full-thickness wound model in mice	Good antibacterial, hemostatic, and anti-inflammatory properties.	2023	[95]

facilitate *coli* and through tion that ugh the rve as a cytokine romoted uction of nt of full- positive lity, thus nts, and specific ed to the elated to negative te these DNA and heir anti-inflammatory and antimicrobial properties [114]. As inorganic agents, they are more stable than their organic agent counterparts. They are also advantageous in their ability to remain within the wound bed for longer periods of time [114][115]. The antimicrobial effects of Zn and ZnO NPs are due to disruption of cell membranes and oxidant injury [114][115]. Zinc also serves as a cofactor for metalloproteinases and other enzymatic complexes, promoting migration of keratinocytes and regeneration of the ECM [114][115]. A previous study examining full-thickness wounds in a rat model showed accelerated and ameliorated healing compared to control with improved re-epithelialization as well as increased collagen deposition and tissue granulation [115]. Moreover, both Zn and ZnO NPs have demonstrated good biocompatibility and low cytotoxicity [114].

Like other NPs, the Zn and ZnO NP effect is dependent on the size, surface-area-to-volume ratio, and concentration of the NPs [116]. Smaller NPs have been shown to be more cytotoxic given their larger surface-area-to-volume ratio, whereas larger NPs demonstrate increased cytocompatibility [117]. In fact, a previous study demonstrated that ZnO NPs are highly compatible with fibroblast cells and promote their growth, migration, and adhesion [100].

Hydrogel Species	Particle Size (Diameter)	Dosage of NP	Rate of Release	Antimicrobial Capability	Cell Type	Cytotoxic Effect	In Vivo Model	In Vivo Findings	Year	Source
		2		sufficient to completely inhibit the growth of *S. aureus* colonies [114][115]		other groups was >80%.		2		
Hyaluronan-polyacrylamide	-	50, 100, 200 µg/mL	At the first stage, the release of Ag^{+} showed an exponential increase for the first ten days, followed by a 'stationary' phase that continued until the 30th day.	exhibited at 200 µg/mL < 1% of the bacteria (*E. coli* and *S. aureus*) survived, compared with the control group. No inhibition zone is found in the 0 µg/mL group, whereas clear inhibition zones were observed for the 50, 100, and 200 µg/mL groups towards *E. coli* and *S. aureus* [118]	3T3 cells	Comparable cell viability compared to control after being cultured for 24 h	*S. aureus* infected full-thickness excisional wound model in rats	The AgNP hydrogel significantly promoted wound healing by improving granulation tissue-formation, angiogenesis, and collagen deposition as well as alleviating inflammation.	2020	[67]
Hyaluronic acid	100 nm	0.5 µM	90% release within 48 h when the pH was reduced from 7.4 to 5.0	Robust antibacterial ratios for both *S. aureus* (95.69%) and *P. aeruginosa* (86.76%) compared to control	HUVECs and L929	>75% cell viability maintained over 3 days	*S. aureus* infected full-thickness excisional wound model in diabetic rats	Accelerated wound closure as well as increased anti-inflammatory, pro-angiogenic, and antibacterial activities were seen in the hydrogel compared to the control.	2022	[68]
Polyvinyl alcohol and gelatin	- [120]	0.1, 0.2, 0.3, 0.4 mM	-	Against *E. coli* and *S. aureus*, a larger inhibition zone compared to the pure hydrogel. [120]	HaCat, LO2 and 293T cells	No inhibitory effects seen, and at low concentrations, a tendency for cell proliferation was noted (5, 10, 15 µg/mL). At higher	*S. aureus* infected full-thickness excisional wounds in mice	Accelerated wound healing, anti-bacterial properties, reduced inflammation, and increased collagen content	2021	[69]

2.6. Iron (Fe) Nanoparticles (FeNP)

Less commonly used in antibacterial wound dressing applications, iron nanoparticles have been shown to induce bacterial death, membrane damage, DNA degradation, and lipid peroxidation [121][122][123]. One study demonstrated high antibacterial activities against *S. aureus* and *E. coli* both in vitro and in an in vivo infected full-thickness excisional wound model in mice where accelerated wound healing and anti-inflammatory properties were observed [121].

2.7. Gallium (Ga) Nanoparticles (GaNP)

Gallium is very infrequently used in wound healing applications. Given that gallium and iron have equal ionic radii, one study hypothesized that the substitution of iron with gallium would impair bacterial iron metabolism and exert an antimicrobial effect [124]. This has previously been observed in vitro, whereby gallium resulted in reduced bacterial survival [124][125][126]. Moreover, given the inability of gallium to be reduced in physiological environments, a property not shared with iron, gallium also disrupts enzyme activity [127]. A 2022 study by Qin et al. demonstrated the good antimicrobial effect of gallium embedded in an alginate-base hydrogel, with good biocompatibility against

Hydrogel Species	Particle Size (Diameter)	Dosage of NP	Rate of Release	Antimicrobial Capability	Cell Type	Cytotoxic Effect	Animal Model	In Vivo Findings	Year	Source
						concentrations, low inhibition was seen, <20% (20, 30, 50, 100 μg/mL)		compared to control		
[129] Propyl methacrylate	-	140, 280, 420 μg/mL	The release amount of Ag^+ in Ag_2S QDs group was much higher than that in NP hydrogel treatment group. Compared with the NP hydrogel-NIR (−) group, the NP hydrogel-NIR (+) group showed a larger release amount of Ag^+ (39.9–84.9 ppb versus 36.6–73.9 ppb), indicating that NIR could accelerate the release of Ag^+. NIR = near-infrared radiation	The inhibition zone diameter of the NP hydrogel group (NP hydrogel-NIR (+) and NP hydrogel-NIR(−)) was significantly larger than that of the control group, with a positive correlation with the NPs concentration against *E. coli* and MRSA. Additionally, the inhibition zone diameter was obviously larger in the NP hydrogel-NIR (+) group than the NP hydrogel-NIR (−) group, demonstrating that the antibacterial ability of the NP hydrogel was enhanced under the assistance of NIR laser irradiation.	NIH 3T3 MEFs, Vero cells	At 420 μg/mL NP concentration, cell survival was still as high as 93.8 ± 3.7% for Vero cells and 96.8 ± 6.2% for NIH 3T3 cells after 48 h of incubation, demonstrating good cytocompatibility	MRSA infected full-thickness excisional wounds in mice	9 days of treatment with NP hydrogel could heal the full-thickness skin defects infected with MRSA with enhanced bacterial clearance, significant collagen deposition, upregulation of VEGF expression, and angiogenesis at the infected sites.	2+ 2022	[70]
Copolymer (PEP)	-	0.75% *w/v*	-	Good antimicrobial activity against MRSA and *E.*	HUVECs, NIH 3T3 MEFs	for HUVEC, cell viability >98% for 200 μg/mL; for NIH-3T3	MRSA infected full-thickness	Rapid wound healing—99.85% of the aggregate wound area was	2019	[71]

collagen [124].

ects. For
ng good
pared to
er study
coli and
l against
as seen
found to
than the

[128]

[130]

2023).

3. Tian, J.; Wong, K.K.; Ho, C.M.; Lok, C.N.; Yu, W.Y.; Che, C.M.; Cliu, J.F.; Tam, P.K. Topical delivery of silver nanoparticles promotes wound healing. ChemMedChem 2007, 2, 129–136.
4. Chen, S.-A.; Chen, H.-M.; Yao, Y.-D.; Hung, C.-F.; Tu, C.-S.; Liang, Y.-J. Topical treatment with anti-oxidants and Au nanoparticles promote healing of diabetic wound through receptor for advance glycation end-products. Eur. J. Pharm. Sci. 2012, 47, 875–883.
5. Tiwari, M.; Narayanan, K.; Thakar, M.B.; Jagani, H.V.; Rao, J.V. Biosynthesis and wound healing activity of copper nanoparticles. IET Nanobiotechnol. 2014, 8, 230–237.
6. Barui, A.K.; Veeriah, V.; Mukherjee, S.; Manna, J.; Patel, A.K.; Patra, S.; Pal, K.; Murali, S.; Rana, R.K.; Chatterjee, S.; et al. Zinc oxide nanoflowers make new blood vessels. Nanoscale 2012, 4, 7861–7869.
7. Kalashnikova, I.; Das, S.; Seal, S. Nanomaterials for wound healing: Scope and advancement. Nanomedicine 2015, 10, 2593–2612.
8. Barroso, A.; Mestre, H.; Ascenso, A.; Simões, S.; Reis, C. Nanomaterials in wound healing: From material sciences to wound healing applications. Nano Sel. 2020, 1, 443–460.

Hydrogel Species	Particle Size (Diameter)	Dosage of NP	Rate of Release	Antimicrobial Capability	Cell Type	Cytotoxic Effect	Animal Model	In Vivo Findings	Year	Source
				coli with inhibition zone of 1.3 cm and 1.4 cm, respectively		cells, cell proliferation was not inhibited over a 3-day span for varying concentrations (50–200 µg/mL)	excisional wounds in rats	healed over the span of 12 days whereas only 54% wound closure was observed for the untreated group.		
Chitosan	60–150 nm	0.5–6.0 mM	-	More obvious zone of inhibition for *S. aureus* compared to *E. coli*. The pure hydrogel alone demonstrated no antibacterial activity	L929 cells	Good cell viability (>90%) for all hydrogels tested	*S. aureus* infected full-thickness excisional wounds in rats	Accelerated the healing process through anti-infection, anti-inflammation, stimulating collagen deposition, and promoting the formation of epithelia and blood vessels compared to control	2022	[72]
Methacrylate gelatin	120 ± 3.392 nm	20 µg/mL	Day 7, the Ag^+ release ratio of the hydrogel was 64.2% ± 4.3% and 70.7% ± 7.8% in solution containing either lysozyme or not, respectively	The numbers of bacterial colony-forming units (CFU) were reduced to 75.3% ± 0.8% for *E. coli*, 88.8% ± 1.3% for *S. aureus*, and 82.1% ± 1.4% for *P. aeruginosa*	NIH 3T3	Excellent biocompatibility observed	*E. coli* and *S. aureus* full-thickness skin burn model in rats	Promotes wound healing by facilitating the regeneration of the epithelial wounds, protecting the wound-rebuilding microvessel network, reducing the inflammation-induced infiltration, enhancing the collagen deposition, and inducing the macrophages to the anti-inflammatory phenotype with noncanonical Wnt signal pathway activated	2022	[73]

17. Singh, B.R.; Singh, B.N.; Singh, A.; Khan, W.; Naqvi, A.H.; Singh, H.B. Mycofabricated biosilver nanoparticles interrupt Pseudomonas aeruginosa quorum sensing systems. Sci. Rep. 2015, 5, 13719.
18. Guide to the Quality and Safety of Tissues and Cells for Human Application—European Directorate for the Quality of Medi-cines & HealthCare—EDQM. European Directorate for the Quality of Medicines & HealthCare. Available online: https://www.edqm.eu/en/guide-to-the-quality-and-safety-of-tissues-and-cells-for-human-application1 (accessed on 20 January 2023).
19. Butler, K.S.; Peeler, D.J.; Casey, B.J.; Dair, B.J.; Elespuru, R.K. Silver nanoparticles: Correlating nanoparticle size and cellular uptake with genotoxicity. Mutagenesis 2015, 30, 577–591.
20. Franková, J.; Pivodová, V.; Vágnerová, H.; Juránová, J.; Ulrichova, J. Effects of silver nanoparticles on primary cell cultures of fibroblasts and keratinocytes in a wound-healing model. J. Appl. Biomater. Funct. Mater. 2016, 14, e137–e142.
21. Wong, K.K.Y.; Cheung, S.O.F.; Huang, L.; Niu, J.; Tao, C.; Ho, C.-M.; Che, C.-M.; Tam, P.K.H. Further Evidence of the Anti-inflammatory Effects of Silver Nanoparticles. Chemmedchem 2009, 4, 1129–1135.

Hydrogel Species	Particle Size (Diameter)	Dosage of NP	Rate of Release	Antimicrobial Capability	Cell Type	Cytotoxic Effect	Animal Model	In Vivo Findings	Year	Source
Gelatin and polyvinyl alcohol	7.4 ± 1.2 nm	-	Sustained release of silver from the hydrogel was detected, and an accumulative 8.99 0.58% of total silver was released after 24 h and 14.98 0.71% was released after 72 h.	>99% of inhibition in all three bacterial strains (99.91 ± 0.52% for *E. coli*, 99.89 ± 0.35% for *S. aureus*, and 99.57 ± 0.73% for MRSA)	L929 cells	Similar biocompatibility compared to pure/blank hydrogel	Full-thickness wounds in rats	Improved antibacterial efficacy, accelerated wound healing and rapid re-epithelialization compared to control	2022	[74]

2 6,

2 als and 531–1551.

25. Chaloupka, K.; Malam, Y.; Seifalian, A.M. Nanosilver as a new generation of nanoproduct in biomedical applications. Trends Biotechnol. 2010, 28, 580–588.
26. Chopra, I. The increasing use of silver-based products as antimicrobial agents: A useful development or a cause for concern? J. Antimicrob. Chemother. 2007, 59, 587–590.
27. Liu, X.; Lee, P.-Y.; Ho, C.-M.; Lui, V.C.H.; Chen, Y.; Che, C.-M.; Tam, P.K.H.; Wong, K.K.Y. Silver Nanoparticles Mediate Differential Responses in Keratinocytes and Fibroblasts during Skin Wound Healing. Chemmedchem 2010, 5, 468–475.
28. GhavamiNejad, A.; Unnithan, A.R.; Sasikala, A.R.K.; Samarikhalaj, M.; Thomas, R.G.; Jeong, Y.Y.; Nasseri, S.; Murugesan, P.; Wu, D.; Park, C.H.; et al. Mussel-Inspired Electrospun Nanofibers Functionalized with Size-Controlled Silver Nanoparticles for Wound Dressing Application. ACS Appl. Mater. Interfaces 2015, 7, 12176–12183.
29. Liu, J.; Sonshine, D.A.; Shervani, S.; Hurt, R.H. Controlled Release of Biologically Active Silver from Nanosilver Surfaces. ACS Nano 2010, 4, 6903–6913.
30. Hamdan, S.; Pastar, I.; Drakulich, S.; Dikici, E.; Tomic-Canic, M.; Deo, S.; Daunert, S. Nanotechnology-Driven Therapeutic Interventions in Wound Healing: Potential Uses and Applications. ACS Central Sci. 2017, 3, 163–175.
31. Ahsan, A.; Farooq, M.A. Therapeutic potential of green synthesized silver nanoparticles loaded PVA hydrogel patches for wound healing. J. Drug Deliv. Sci. Technol. 2019, 54, 101308.
32. Anjum, S.; Gupta, A.; Sharma, D.; Gautam, D.; Bhan, S.; Sharma, A.; Kapil, A.; Gupta, B. Development of novel wound care systems based on nanosilver nanohydrogels of polymethacrylic acid with Aloe vera and curcumin. Mater. Sci. Eng. C 2016, 64, 157–166.
33. Bharathi, S.; Ramesh, B.; Kumaran, S.; Radhakrishnan, M.; Saravanan, D.; Pugazhvendan, S.R.; Nalinasundari, M.S. Development of nanobiomaterial for wound healing based on silver nanoparticles loaded on chitosan hydrogel. 3 Biotech 2021, 11, 490.
34. Bhubhanil, S.; Talodthaisong, C.; Khongkow, M.; Namdee, K.; Wongchitrat, P.; Yingmema, W.; Hutchison, J.A.; Lapmanee, S.; Kulchat, S. Enhanced wound healing properties of guar

gum/curcumin-stabilized silver nanoparticle hydrogels. Sci. Rep. 2021, 11, 21836.

35. Chen, Q.; Li, S.; Zhao, W.; Zhao, C. A rapid-triggered approach towards antibacterial hydrogel wound dressing with synergic photothermal and sterilization profiles. Biomater. Adv. 2022, 138, 212873.
36. Lin, Z.; Fan, D.; Li, G.; He, L.; Qin, X.; Zhao, B.; Wang, Q.; Liang, W. Antibacterial, Adhesive, and Conductive Hydrogel for Diabetic Wound Healing. Macromol. Biosci. 2022, 23, 2200349.
37. Sharifi, E.; Sadati, S.A.; Yousefiasl, S.; Sartorius, R.; Zafari, M.; Rezakhani, L.; Alizadeh, M.; Zare, E.N.; Omidghaemi, S.; Ghanavatinejad, F.; et al. Cell loaded hydrogel containing Ag-doped bioactive glass–ceramic nanoparticles as skin substitute: Antibacterial properties, immune response, and scarless cutaneous wound regeneration. Bioeng. Transl. Med. 2022, 7, e10386.
38. Chinnasamy, G.; Chandrasekharan, S.; Koh, T.W.; Bhatnagar, S. Synthesis, Characterization, Antibacterial and Wound Healing Efficacy of Silver Nanoparticles From Azadirachta indica. Front. Microbiol. 2021, 12, 611560.
39. Choudhary, M.; Chhabra, P.; Tyagi, A.; Singh, H. Scar free healing of full thickness diabetic wounds: A unique combination of silver nanoparticles as antimicrobial agent, calcium alginate nanoparticles as hemostatic agent, fresh blood as nutrient/growth factor supplier and chitosan as base matrix. Int. J. Biol. Macromol. 2021, 178, 41–52.
40. De Lima, G.G.; De Lima, D.W.F.; De Oliveira, M.J.A.; Lugão, A.B.; Alcântara, M.T.S.; Devine, D.M.; De Sá, M.J.C. Synthesis and in Vivo Behavior of PVP/CMC/Agar Hydrogel Membranes Impregnated with Silver Nanoparticles for Wound Healing Applications. ACS Appl. Bio Mater. 2018, 1, 1842–1852.
41. Cao, C.; Yang, N.; Zhao, Y.; Yang, D.; Hu, Y.; Yang, D.; Song, X.; Wang, W.; Dong, X. Biodegradable hydrogel with thermo-response and hemostatic effect for photothermal enhanced anti-infective therapy. Nano Today 2021, 39, 101165.
42. Deng, P.; Chen, F.; Zhang, H.; Chen, Y.; Zhou, J. Conductive, Self-Healing, Adhesive, and Antibacterial Hydrogels Based on Lignin/Cellulose for Rapid MRSA-Infected Wound Repairing. ACS Appl. Mater. Interfaces 2021, 13, 52333–52345.
43. Diniz, F.R.; Maia, R.C.A.P.; Andrade, L.R.; Andrade, L.N.; Chaud, M.V.; Da Silva, C.F.; Corrêa, C.B.; de Albuquerque Junior, R.L.C.; Da Costa, L.P.; Shin, S.R.; et al. Silver Nanoparticles-Composing Alginate/Gelatine Hydrogel Improves Wound Healing In Vivo. Nanomaterials 2020, 10, 390.
44. Garg, S.; Chandra, A.; Mazumder, A.; Mazumder, R. Green synthesis of silver nanoparticles using Arnebia nobilis root extract and wound healing potential of its hydrogel. Asian J. Pharm. 2014, 8, 95.

45. GhavamiNejad, A.; Park, C.H.; Kim, C.S. In Situ Synthesis of Antimicrobial Silver Nanoparticles within Antifouling Zwitterionic Hydrogels by Catecholic Redox Chemistry for Wound Healing Application. Biomacromolecules 2016, 17, 1213–1223.
46. Haidari, H.; Bright, R.; Strudwick, X.L.; Garg, S.; Vasilev, K.; Cowin, A.J.; Kopecki, Z. Multifunctional ultrasmall AgNP hydrogel accelerates healing of S. aureus infected wounds. Acta Biomater. 2021, 128, 420–434.
47. Jiang, Y.; Huang, J.; Wu, X.; Ren, Y.; Li, Z.; Ren, J. Controlled release of silver ions from AgNPs using a hydrogel based on konjac glucomannan and chitosan for infected wounds. Int. J. Biol. Macromol. 2020, 149, 148–157.
48. Kong, C.; Chen, S.; Ge, W.; Zhao, Y.; Xu, X.; Wang, S.; Zhang, J. Riclin-Capped Silver Nanoparticles as an Antibacterial and Anti-Inflammatory Wound Dressing. Int. J. Nanomed. 2022, 17, 2629–2641.
49. Lee, Y.-H.; Hong, Y.-L.; Wu, T.-L. Novel silver and nanoparticle-encapsulated growth factor co-loaded chitosan composite hydrogel with sustained antimicrobility and promoted biological properties for diabetic wound healing. Mater. Sci. Eng. C Mater. Biol. Appl. 2021, 118, 111385.
50. Li, B.; Li, H.; Yang, H.; Shu, Y.; Li, K.; Chen, K.; Xiao, W.; Liao, X. Preparation and antibacterial properties of an /GelMA composite hydrogel. Biomed. Mater. 2022, 17, 025005.
51. Liu, K.; Dai, L.; Li, C. A lignocellulose-based nanocomposite hydrogel with pH-sensitive and potent antibacterial activity for wound healing. Int. J. Biol. Macromol. 2021, 191, 1249–1254.
52. Liu, R.; Dai, L.; Si, C.; Zeng, Z. Antibacterial and hemostatic hydrogel via nanocomposite from cellulose nanofibers. Carbohydr. Polym. 2018, 195, 63–70.
53. Liu, Y.; Fan, J.; Lv, M.; She, K.; Sun, J.; Lu, Q.; Han, C.; Ding, S.; Zhao, S.; Wang, G.; et al. Photocrosslinking silver nanoparticles–aloe vera–silk fibroin composite hydrogel for treatment of full-thickness cutaneous wounds. Regen. Biomater. 2021, 8, rbab048.
54. Lustosa, A.K.M.F.; Oliveira, A.C.D.J.; Quelemes, P.V.; Plácido, A.; Da Silva, F.V.; Oliveira, I.S.; De Almeida, M.P.; Amorim, A.D.G.N.; Delerue-Matos, C.; Oliveira, R.D.C.M.D.; et al. In Situ Synthesis of Silver Nanoparticles in a Hydrogel of Carboxymethyl Cellulose with Phthalated-Cashew Gum as a Promising Antibacterial and Healing Agent. Int. J. Mol. Sci. 2017, 18, 2399.
55. Qiu, Y.; Sun, X.; Lin, X.; Yi, W.; Jiang, J. An injectable metal nanoparticle containing cellulose derivative-based hydrogels: Evaluation of antibacterial and in vitro-vivo wound healing activity in children with burn injuries. Int. Wound J. 2021, 19, 666–678.
56. Mei, J.; Zhou, J.; Kong, L.; Dai, Y.; Zhang, X.; Song, W.; Zhu, C. An injectable photo-cross-linking silk hydrogel system augments diabetic wound healing in orthopaedic surgery through spatiotemporal immunomodulation. J. Nanobiotechnol. 2022, 20, 232.

57. Martínez-Higuera, A.; Rodríguez-Beas, C.; Villalobos-Noriega, J.M.A.; Arizmendi-Grijalva, A.; Ochoa-Sánchez, C.; Larios-Rodríguez, E.; Martínez-Soto, J.M.; Rodríguez-León, E.; Ibarra-Zazueta, C.; Mora-Monroy, R.; et al. Hydrogel with silver nanoparticles synthesized by Mimosa tenuiflora for second-degree burns treatment. Sci. Rep. 2021, 11, 11312.

58. Masood, N.; Ahmed, R.; Tariq, M.; Ahmed, Z.; Masoud, M.S.; Ali, I.; Asghar, R.; Andleeb, A.; Hasan, A. Silver nanoparticle impregnated chitosan-PEG hydrogel enhances wound healing in diabetes induced rabbits. Int. J. Pharm. 2019, 559, 23–36.

59. Mugade, M.; Patole, M.; Pokharkar, V. Bioengineered mannan sulphate capped silver nanoparticles for accelerated and targeted wound healing: Physicochemical and biological investigations. Biomed. Pharmacother. 2017, 91, 95–110.

60. Shi, G.; Chen, W.; Zhang, Y.; Dai, X.; Zhang, X.; Wu, Z. An Antifouling Hydrogel Containing Silver Nanoparticles for Modulating the Therapeutic Immune Response in Chronic Wound Healing. Langmuir 2018, 35, 1837–1845.

61. Hu, J.; Tao, M.; Sun, F.; Chen, C.; Chen, G.; Wang, G. Multifunctional hydrogel based on dopamine-modified hyaluronic acid, gelatin and silver nanoparticles for promoting abdominal wall defect repair. Int. J. Biol. Macromol. 2022, 222, 55–64.

62. Ren, Y.; Ailierken, A.; Zhao, L.; Lin, Z.; Jiang, J.; Li, B.; Wang, J.; Hua, J.; Tu, Q. hUC-MSCs lyophilized powder loaded polysaccharide ulvan driven functional hydrogel for chronic diabetic wound healing. Carbohydr. Polym. 2022, 288, 119404.

63. Li, Y.; Fu, R.; Duan, Z.; Zhu, C.; Fan, D. Mussel-inspired adhesive bilayer hydrogels for bacteria-infected wound healing via NIR-enhanced nanozyme therapy. Colloids Surfaces B Biointerfaces 2021, 210, 112230.

64. Kong, F.; Fan, C.; Yang, Y.; Lee, B.H.; Wei, K. 5-hydroxymethylfurfural-embedded poly (vinyl alcohol)/sodium alginate hybrid hydrogels accelerate wound healing. Int. J. Biol. Macromol. 2019, 138, 933–949.

65. He, H.; Xia, D.-L.; Chen, Y.-P.; Li, X.-D.; Chen, C.; Wang, Y.-F.; Shen, L.; Hu, Y.-L.; Gu, H.-Y. Evaluation of a two-stage antibacterial hydrogel dressing for healing in an infected diabetic wound: ANTIBACTERIAL HYDROGEL DRESSING FOR DIABETIC WOUND HEALING. J. Biomed. Mater. Res. Part B Appl. Biomater. 2016, 105, 1808–1817.

66. Song, S.; Liu, Z.; Abubaker, M.A.; Ding, L.; Zhang, J.; Yang, S.; Fan, Z. Antibacterial polyvinyl alcohol/bacterial cellulose/nano-silver hydrogels that effectively promote wound healing. Mater. Sci. Eng. C 2021, 126, 112171.

67. Tang, Q.; Chen, C.; Jiang, Y.; Huang, J.; Liu, Y.; Nthumba, P.M.; Gu, G.; Wu, X.; Zhao, Y.; Ren, J. Engineering an adhesive based on photosensitive polymer hydrogels and silver nanoparticles for wound healing. J. Mater. Chem. B 2020, 8, 5756–5764.

68. Deng, M.; Wu, Y.; Ren, Y.; Song, H.; Zheng, L.; Lin, G.; Wen, X.; Tao, Y.; Kong, Q.; Wang, Y. Clickable and smart drug delivery vehicles accelerate the healing of infected diabetic wounds. J. Control. Release 2022, 350, 613–629.
69. Xiao, L.; Hui, F.; Tian, T.; Yan, R.; Xin, J.; Zhao, X.; Jiang, Y.; Zhang, Z.; Kuang, Y.; Li, N.; et al. A Novel Conductive Antibacterial Nanocomposite Hydrogel Dressing for Healing of Severely Infected Wounds. Front. Chem. 2021, 9, 787886.
70. Du, T.; Xiao, Z.; Cao, J.; Wei, L.; Li, C.; Jiao, J.; Song, Z.; Liu, J.; Du, X.; Wang, S. NIR-activated multi-hit therapeutic Ag2S quantum dot-based hydrogel for healing of bacteria-infected wounds. Acta Biomater. 2022, 145, 88–105.
71. Yan, X.; Fang, W.-W.; Xue, J.; Sun, T.-C.; Dong, L.; Zha, Z.; Qian, H.; Song, Y.-H.; Zhang, M.; Gong, X.; et al. Thermoresponsive in Situ Forming Hydrogel with Sol–Gel Irreversibility for Effective Methicillin-Resistant Staphylococcus aureus Infected Wound Healing. ACS Nano 2019, 13, 10074–10084.
72. Zhao, F.; Liu, Y.; Song, T.; Zhang, B.; Li, D.; Xiao, Y.; Zhang, X. A chitosan-based multifunctional hydrogel containing in situ rapidly bioreduced silver nanoparticles for accelerating infected wound healing. J. Mater. Chem. B 2022, 10, 2135–2147.
73. Xiong, Y.; Xu, Y.; Zhou, F.; Hu, Y.; Zhao, J.; Liu, Z.; Zhai, Q.; Qi, S.; Zhang, Z.; Chen, L. Bio-functional hydrogel with antibacterial and anti-inflammatory dual properties to combat with burn wound infection. Bioeng. Transl. Med. 2022, 8, e10373.
74. Xiang, J.; Bai, Y.; Huang, Y.; Lang, S.; Li, J.; Ji, Y.; Peng, B.; Liu, G. A zwitterionic silver nanoparticle-incorporating injectable hydrogel with a durable and efficient antibacterial effect for accelerated wound healing. J. Mater. Chem. B 2022, 10, 7979–7994.
75. Guo, R.; Song, Y.; Wang, G.; Murray, R.W. Does Core Size Matter in the Kinetics of Ligand Exchanges of Monolayer-Protected Au Clusters? J. Am. Chem. Soc. 2005, 127, 2752–2757.
76. BarathManiKanth, S.; Kalishwaralal, K.; Sriram, M.; Pandian, S.R.K.; Youn, H.S.; Eom, S.; Gurunathan, S. RAesneatrcih-oxidant effect of gold nanoparticles restrains hyperglycemic conditions in diabetic mice. J. Nanobiotechnol. 2010, 8, 16.
77. Ghosh, P.; Han, G.; De, M.; Kim, C.K.; Rotello, V.M. Gold nanoparticles in delivery applications. Adv. Drug Deliv. Rev. 2008, 60, 1307–1315.
78. Zain, N.M.; Stapley, A.; Shama, G. Green synthesis of silver and copper nanoparticles using ascorbic acid and chitosan for antimicrobial applications. Carbohydr. Polym. 2014, 112, 195–202.
79. Muller, A.P.; Ferreira, G.K.; Pires, A.J.; Silveira, G.D.B.; de Souza, D.L.; Brandolfi, J.D.A.; de Souza, C.T.; Paula, M.M.; Silveira, P.C.L. Gold nanoparticles prevent cognitive deficits, oxidative stress and inflammation in a rat model of sporadic dementia of Alzheimer’s type. Mater. Sci. Eng. C 2017, 77, 476–483.

80. Li, X.; Wang, H.; Rong, H.; Li, W.; Luo, Y.; Tian, K.; Quan, D.; Wang, Y.; Jiang, L. Effect of composite SiO 2 @AuNPs on wound healing: In vitro and vivo studies. J. Colloid Interface Sci. 2015, 445, 312–319.
81. Victor, E.G.; Silveira, P.C.; Possato, J.C.; da Rosa, G.L.; Munari, U.B.; de Souza, C.T.; Pinho, R.A.; da Silva, L.; Streck, E.L.; Paula, M.M. Pulsed ultrasound associated with gold nanoparticle gel reduces oxidative stress parameters and expression of pro-inflammatory molecules in an animal model of muscle injury. J. Nanobiotechnol. 2012, 10, 11.
82. Medhe, S.; Bansal, P.; Srivastava, M.M. Enhanced antioxidant activity of gold nanoparticle embedded 3,6-dihydroxyflavone: A combinational study. Appl. Nanosci. 2014, 4, 153–161.
83. Leu, J.-G.; Chen, S.-A.; Chen, H.-M.; Wu, W.-M.; Hung, C.-F.; Yao, Y.-D.; Tu, C.-S.; Liang, Y.-J. The effects of gold nanoparticles in wound healing with antioxidant epigallocatechin gallate and α-lipoic acid. Nanomed. Nanotechnol. Biol. Med. 2012, 8, 767–775.
84. Esumi, K.; Houdatsu, H.; Yoshimura, T. Antioxidant Action by Gold−PAMAM Dendrimer Nanocomposites. Langmuir 2004, 20, 2536–2538.
85. Rattanata, N.; Daduang, S.; Wongwattanakul, M.; Leelayuwat, C.; Limpaiboon, T.; Lekphrom, R.; Sandee, A.; Boonsiri, P.; Chio-Srichan, S.; Daduang, J. Gold Nanoparticles Enhance the Anticancer Activity of Gallic Acid against Cholangiocarcinoma Cell Lines. Asian Pac. J. Cancer Prev. 2015, 16, 7143–7147.
86. Cheng, H.; Lai, G.; Fu, L.; Zhang, H.; Yu, A. Enzymatically catalytic deposition of gold nanoparticles by glucose oxidase-functionalized gold nanoprobe for ultrasensitive electrochemical immunoassay. Biosens. Bioelectron. 2015, 71, 353–358.
87. Haupenthal, D.P.D.S.; Mendes, C.; Silveira, G.D.B.; Zaccaron, R.P.; Corrêa, M.E.A.B.; Nesi, R.T.; Pinho, R.; Paula, M.M.D.S.; Silveira, P.C.L. Effects of treatment with gold nanoparticles in a model of acute pulmonary inflammation induced by lipopolysaccharide. J. Biomed. Mater. Res. Part A 2019, 108, 103–115.
88. Arvizo, R.R.; Bhattacharyya, S.; Kudgus, R.A.; Giri, K.; Bhattacharya, R.; Mukherjee, P. Intrinsic therapeutic applications of noble metal nanoparticles: Past, present and future. Chem. Soc. Rev. 2012, 41, 2943–2970.
89. Tuhin, R.H.; Begum, M.M.; Rahman, S.; Karim, R.; Begum, T.; Ahmed, S.U.; Mostofa, R.; Hossain, A.; Abdel-Daim, M.; Begum, R. Wound healing effect of Euphorbia hirta linn. (Euphorbiaceae) in alloxan induced diabetic rats. BMC Complement. Altern. Med. 2017, 17, 423.
90. Batool, Z.; Muhammad, G.; Iqbal, M.M.; Aslam, M.S.; Raza, M.A.; Sajjad, N.; Abdullah, M.; Akhtar, N.; Syed, A.; Elgorban, A.M.; et al. Hydrogel assisted synthesis of gold nanoparticles with enhanced microbicidal and in vivo wound healing potential. Sci. Rep. 2022, 12, 6575.

91. Kaul, S.; Sagar, P.; Gupta, R.; Garg, P.; Priyadarshi, N.; Singhal, N.K. Mechanobactericidal, Gold Nanostar Hydrogel-Based Bandage for Bacteria-Infected Skin Wound Healing. ACS Appl. Mater. Interfaces 2022, 14, 44084–44097.
92. Mahmoud, N.N.; Hikmat, S.; Abu Ghith, D.; Hajeer, M.; Hamadneh, L.; Qattan, D.; Khalil, E.A. Gold nanoparticles loaded into polymeric hydrogel for wound healing in rats: Effect of nanoparticles' shape and surface modification. Int. J. Pharm. 2019, 565, 174–186.
93. Shang, K.; Tao, L.; Jiang, S.; Yan, J.; Hu, S.; Yang, G.; Ma, C.; Cheng, S.; Wang, X.; Yin, J. Highly flexible hydrogel dressing with efficient antibacterial, antioxidative, and wound healing performances. Biomater. Sci. 2022, 10, 1373–1383.
94. Pérez-Rafael, S.; Ivanova, K.; Stefanov, I.; Puiggalí, J.; del Valle, L.J.; Todorova, K.; Dimitrov, P.; Hinojosa-Caballero, D.; Tzanov, T. Nanoparticle-driven self-assembling injectable hydrogels provide a multi-factorial approach for chronic wound treatment. Acta Biomater. 2021, 134, 131–143.
95. Zhao, P.; Feng, Y.; Zhou, Y.; Tan, C.; Liu, M. nanotubes-chitin composite hydrogel with antibacterial and hemostatic activity for wound healing. Bioact. Mater. 2023, 20, 355–367.
96. Melamed, E.; Kiambi, P.; Okoth, D.; Honigber, I.; Tamir, E.; Borkow, G. Healing of Chronic Wounds by Copper Oxide-Impregnated Wound Dressings—Case Series. Medicina 2021, 57, 296.
97. Baek, J.H.; Yoo, M.A.; Koh, J.S.; Borkow, G. Reduction of facial wrinkles depth by sleeping on copper oxide-containing pillowcases: A double blind, placebo controlled, parallel, randomized clinical study: Wrinkles reduction with copper pillowcases. J. Cosmet. Dermatol. 2012, 11, 193–200.
98. Dykes, P. Increase in skin surface elasticity in normal volunteer subjects following the use of copper oxide impregnated socks. Ski. Res. Technol. 2014, 21, 272–277.
99. Barani, M.; Rahdar, A.; Mukhtar, M.; Razzaq, S.; Qindeel, M.; Olam, S.A.H.; Paiva-Santos, A.C.; Ajalli, N.; Sargazi, S.; Balakrishnan, D.; et al. Recent application of cobalt ferrite nanoparticles as a theranostic agent. Mater. Today Chem. 2022, 26, 101131.
100. Manuja, A.; Raguvaran, R.; Kumar, B.; Kalia, A.; Tripathi, B. Accelerated healing of full thickness excised skin wound in rabbits using single application of alginate/acacia based nanocomposites of ZnO nanoparticles. Int. J. Biol. Macromol. 2020, 155, 823–833.
101. El-Abeid, S.E.; Ahmed, Y.; Daròs, J.-A.; Mohamed, M.A. Reduced Graphene Oxide Nanosheet-Decorated Copper Oxide Nanoparticles: A Potent Antifungal Nanocomposite against Fusarium Root Rot and Wilt Diseases of Tomato and Pepper Plants. Nanomaterials 2020, 10, 1001.
102. Hopkins, R.G.; Failla, M.L. Copper Deficiency Reduces Interleukin-2 (IL-2) Production and IL-2 mRNA in Human T-Lymphocytes. J. Nutr. 1997, 127, 257–262.

103. Kornblatt, A.P.; Nicoletti, V.G.; Travaglia, A. The neglected role of copper ions in wound healing. J. Inorg. Biochem. 2016, 161, 1–8.
104. Uauy, R.; Olivares, M.; Gonzalez, M. Essentiality of copper in humans. Am. J. Clin. Nutr. 1998, 67, S952–S959.
105. Borkow, G.; Gabbay, J.; Dardik, R.; Eidelman, A.I.; Lavie, Y.; Grunfeld, Y.; Ikher, S.; Huszar, M.; Zatcoff, R.C.; Marikovsky, M. Molecular mechanisms of enhanced wound healing by copper oxide-impregnated dressings. Wound Repair Regen. 2010, 18, 266–275.
106. Quaranta, D.; Krans, T.; Santo, C.E.; Elowsky, C.G.; Domaille, D.W.; Chang, C.J.; Grass, G. Mechanisms of Contact-Mediated Killing of Yeast Cells on Dry Metallic Copper Surfaces. Appl. Environ. Microbiol. 2011, 77, 416–426.
107. Palza, H. Antimicrobial Polymers with Metal Nanoparticles. Int. J. Mol. Sci. 2015, 16, 2099–2116.
108. Zhou, M.; Tian, M.; Li, C. Copper-Based Nanomaterials for Cancer Imaging and Therapy. Bioconjugate Chem. 2016, 27, 1188–1199.
109. Grigore, M.E.; Biscu, E.R.; Holban, A.M.; Gestal, M.C.; Grumezescu, A.M. Methods of Synthesis, Properties and Biomedical Applications of CuO Nanoparticles. Pharmaceuticals 2016, 9, 75.
110. Zhang, Q.; Zhang, K.; Xu, D.; Yang, G.; Huang, H.; Nie, F.; Liu, C.; Yang, S. CuO nanostructures: Synthesis, characterization, growth mechanisms, fundamental properties, and applications. Prog. Mater. Sci. 2013, 60, 208–337.
111. Ungur, G.; Hruza, J. Influence of copper oxide on the formation of polyurethane nanofibers via electrospinning. Fibers Polym. 2015, 16, 621–628.
112. Xiao, Y.; Reis, L.A.; Feric, N.; Knee, E.J.; Gu, J.; Cao, S.; Laschinger, C.; Londono, C.; Antolovich, J.; McGuigan, A.P.; et al. Diabetic wound regeneration using peptide-modified hydrogels to target re-epithelialization. Proc. Natl. Acad. Sci. USA 2016, 113, E5792–E5801.
113. Marrazzo, P.; O'leary, C. Repositioning Natural Antioxidants for Therapeutic Applications in Tissue Engineering. Bioengineering 2020, 7, 104.
114. Jaiswal, M.; Koul, V.; Dinda, A.K. In vitro and in vivo investigational studies of a nanocomposite-hydrogel-based dressing with a silver-coated chitosan wafer for full-thickness skin wounds. J. Appl. Polym. Sci. 2016, 133, 21.
115. Yadid, M.; Feiner, R.; Dvir, T. Gold Nanoparticle-Integrated Scaffolds for Tissue Engineering and Regenerative Medicine. Nano Lett. 2019, 19, 2198–2206.
116. Czyżowska, A.; Barbasz, A. A review: Zinc oxide nanoparticles–friends or enemies? Int. J. Environ. Health Res. 2020, 32, 885–901.

117. Kaushik, M.; Niranjan, R.; Thangam, R.; Madhan, B.; Pandiyarasan, V.; Ramachandran, C.; Oh, D.-H.; Venkatasubbu, G.D. Investigations on the antimicrobial activity and wound healing potential of ZnO nanoparticles. Appl. Surf. Sci. 2019, 479, 1169–1177.

118. Archana, D.; Singh, B.K.; Dutta, J.; Dutta, P. Chitosan-PVP-nano silver oxide wound dressing: In vitro and in vivo evaluation. Int. J. Biol. Macromol. 2015, 73, 49–57.

119. Zhang, F.; Chan, S.-W.; Spanier, J.E.; Apak, E.; Jin, Q.; Robinson, R.D.; Herman, I.P. Cerium oxide nanoparticles: Size-selective formation and structure analysis. Appl. Phys. Lett. 2002, 80, 127–129.

120. Wang, Q.; Qiu, W.; Li, M.; Li, N.; Li, X.; Qin, X.; Wang, X.; Yu, J.; Li, F.; Huang, L.; et al. Mussel-inspired multifunctional hydrogel dressing with hemostasis, hypoglycemic, photothermal antibacterial properties on diabetic wounds. Biomater. Sci. 2022, 10, 4796–4814.

121. Xu, Z.; Gao, Z.; Lu, J.; Wang, T.; Wang, W.; Fan, L.; Xi, J.; Han, B. Ferrous iron-induced formation of glycyrrhizic acid hydrogels for Staphylococcus aureus-infected wound healing. Colloids Surf. B Biointerfaces 2023, 221, 112977.

122. Xi, J.; An, L.; Huang, Y.; Jiang, J.; Wang, Y.; Wei, G.; Xu, Z.; Fan, L.; Gao, L. Ultrasmall FeS2 Nanoparticles-Decorated Carbon Spheres with Laser-Mediated Ferrous Ion Release for Antibacterial Therapy. Small 2021, 17, e2005473.

123. Shen, X.; Ma, R.; Huang, Y.; Chen, L.; Xu, Z.; Li, D.; Meng, X.; Fan, K.; Xi, J.; Yan, X.; et al. Nano-decocted ferrous polysulfide coordinates ferroptosis-like death in bacteria for anti-infection therapy. Nano Today 2020, 35, 100981.

124. Qin, J.; Li, M.; Yuan, M.; Shi, X.; Song, J.; He, Y.; Mao, H.; Kong, D.; Gu, Z. Gallium(III)-Mediated Dual-Cross-Linked Alginate Hydrogels with Antibacterial Properties for Promoting Infected Wound Healing. ACS Appl. Mater. Interfaces 2022, 14, 22426–22442.

125. Goss, C.H.; Kaneko, Y.; Khuu, L.; Anderson, G.D.; Ravishankar, S.; Aitken, M.L.; Lechtzin, N.; Zhou, G.; Czyz, D.M.; McLean, K.; et al. Gallium disrupts bacterial iron metabolism and has therapeutic effects in mice and humans with lung infections. Sci. Transl. Med. 2018, 10, eaat7520.

126. Lemire, J.A.; Harrison, J.J.; Turner, R.J. Antimicrobial activity of metals: Mechanisms, molecular targets and applications. Nat. Rev. Microbiol. 2013, 11, 371–384.

127. Choi, S.-R.; Switzer, B.; Britigan, B.E.; Narayanasamy, P. Gallium Porphyrin and Gallium Nitrate Synergistically Inhibit Mycobacterial Species by Targeting Different Aspects of Iron/Heme Metabolism. ACS Infect. Dis. 2020, 6, 2582–2591.

128. Liu, X.; Zhou, S.; Cai, B.; Wang, Y.; Deng, D.; Wang, X. An injectable and self-healing hydrogel with antibacterial and angiogenic properties for diabetic wound healing. Biomater. Sci. 2022, 10, 3480–3492.

129. Zhang, Y.; Liu, X.; Li, Z.; Zhu, S.; Yuan, X.; Cui, Z.; Yang, X.; Chu, P.K.; Wu, S. Nano Ag/ZnO-Incorporated Hydroxyapatite Composite Coatings: Highly Effective Infection Prevention and Excellent Osteointegration. ACS Appl. Mater. Interfaces 2018, 10, 1266–1277.

130. Mao, C.; Xiang, Y.; Liu, X.; Cui, Z.; Yang, X.; Yeung, K.W.K.; Pan, H.; Wang, X.; Chu, P.K.; Wu, S. Photo-Inspired Antibacterial Activity and Wound Healing Acceleration by Hydrogel Embedded with Ag//ZnO Nanostructures. ACS Nano 2017, 11, 9010–9021.